

Twist Angle Dependent Ultrafast Transient Dynamics of MoSe₂/WSe₂ van der Waals Heterostructures beyond the Exciton Mott Transition

Vikas Arora^{1,2}, Pramoda K Nayak^{3,4}, D. V. S. Muthu¹, A K Sood^{*1,2}

June 12, 2025

¹*Department of Physics, Indian Institute of Science, Bangalore 560012, India*

²*Centre for Ultrafast Laser Applications, Indian Institute of Science, Bangalore 560012, India*

³*2D Materials Research and Innovation Group, Department of Physics, Indian Institute of Technology Madras, Chennai 600036, India*

⁴*Centre for Nano and Materials Sciences, Jain (Deemed-to-be University), Jain Global Campus, Kanakpura, Bangalore 562112, Karnataka, India*

Keywords: van der Waals Heterostructure, Raman spectroscopy, optical pump-optical probe spectroscopy, ultrafast carrier relaxation dynamics, interlayer excitons, exciton Mott's transition.

Abstract

Two-dimensional van der Waals heterostructures (HS) exhibit twist-angle (θ) dependent inter-layer charge transfer, driven by moiré potential that tunes the electronic band structure with varying θ . Apart from the magic angles of $\sim 3^\circ$ and $\sim 57.5^\circ$ that show flat valence bands (twisted WSe₂ bilayer), the commensurate angles of 21.8° and 38.2° reveal the Umklapp light coupling of inter-layer excitons. We report our results on non-degenerate optical pump-optical probe spectroscopy of MoSe₂/WSe₂ HS at large twist angles under high photoexcitation densities above the Mott transition threshold, generating interlayer localized charge carriers. We show that the recombination time of electrons and holes is minimum at the commensurate angles. The strength of non-radiative interlayer Auger recombination also shows a minimum at the commensurate angles. The fluence

dependence of interlayer carrier recombination time suggests additional relaxation channels near the commensurate angles. This study emphasizes the significance of the large twist angle of HS in developing transition metal dichalcogenides-based optoelectronic devices.

Introduction

Two-dimensional materials such as graphene, transition metal dichalcogenides (TMDs), and h-BN, along with their heterostructures (HS), show many exciting physical properties. For example, in the case of TMDs, properties such as the large binding energy of excitons [1–3], a strong non-linear optical response [4–6] and spin-valley coupling [7, 8] are exhibited. For the heterobilayers MoX_2/WX_2 , the energy levels are decided by d orbitals of transition metal. The $5d$ orbital of W is higher than that of the $4d$ orbital of Mo, and hence, the conduction band minima and valence band maxima of tungsten are higher than that of molybdenum. This creates a staggered or type-II band alignment [9, 10]. This alignment facilitates ultrafast charge transfer between the layers, generation of interlayer exciton with longer decay times [11, 12], and energy transfer among the layers [3, 13]. The optoelectronic properties have been shown to depend on the twist angle between the layers. The twist between the two layers gives rise to a periodic array of potential minima known as the moiré pattern [14–17]. At low temperatures and low twist angles, the multiple sharp peaks superimposed over the photoluminescence (PL) spectra denotes the interlayer excitons trapped in moiré quantum wells [18, 19]. Self-organized quantum dots are observed in $\text{MoSe}_2/\text{WSe}_2$ and MoS_2/WS_2 HS for twist angles less than 0.5° [20]. For $\text{WS}_2/\text{MoSe}_2$ HS, twist angle tunes the moiré reciprocal lattice and hence the properties of moiré excitons such as oscillator strength and inter/intralayer mixing [21]. In a twisted WSe_2 bilayer, flat top moiré valence bands are observed at magic angles of $\sim 3^\circ$ and $\sim 57.5^\circ$ [22–24]. While small twist angles reveal the properties of moiré excitons, large twist angles describe the characteristics of interlayer excitons.

Nayak *et al.* [10] observed the quenching of photoluminescence for the $\text{MoSe}_2/\text{WSe}_2$ HS for all the twist angles as compared to constituent monolayers. A redshift in PL energy of up to ~ 100 meV has been observed in HS $\text{WSe}_2/\text{MoSe}_2$ depending on the twist angle [25, 26]. It has been reported that the PL intensity is two orders lesser for $\theta = 20^\circ$ as compared to $\theta = 2^\circ$ for $\text{MoSe}_2/\text{WSe}_2$ HS [27]. The interlayer distance and binding energy of interlayer exciton are twist-dependent and are maximum at 30° , as revealed by the PL studies [28, 29]. Yu *et al.* have shown that the interlayer excitons undergo Umklapp recombination near the commensurate twist angles of 21.8° and 38.2° [27, 30]. The additional

channel for recombination of interlayer excitons at these particular angles predicts anomalous relaxation dynamics for the HS. The significance of the commensurate angle 21.8° has been emphasized in recent reports on HS $\text{MoS}_2/\text{MoSe}_2$, demonstrating the highest thermoelectric performance ($ZT = 2.96$ at $T = 700$ K) [31] and recording the highest indirect bandgap [32].

A recent report on ultrafast electron diffraction of $\text{MoSe}_2/\text{WSe}_2$ HS indicates that interlayer heat transfer occurs on a ~ 20 ps timescale, mediated by nonthermal phonons followed by interlayer charge transfer and scattering [33]. The ultrafast transient absorption spectroscopy of TMDs HS has shown that the interlayer charge transfer happens on the order of 100 fs time scale [34–39]. A slight variation in geometry or twist angle of the HS can vary the charge transfer time from 100 fs to 1 ps [3, 40, 41]. Zhu *et al.* have reported the recombination time for interlayer exciton in twisted $\text{WSe}_2/\text{MoS}_2$ HS, varying from 40 ps to 3 ns for twist angles between 0° and 30° , and attributed this variation to non-radiative defect-mediated recombination [42]. In this study, no systematic twist-angle dependence of recombination time was observed. We note that these experiments were performed at a fluence of $\sim 10^{11} \text{ cm}^{-2}$, which is below the exciton Mott transition (MT) [42]. The Mott transition occurs above a certain photoexcitation density, where the distance between excitons becomes smaller than their radius, thus screening the Coulomb interactions between electrons and holes resulting in an unbounded electron-hole plasma [43, 44]. The Mott transition of excitons has been observed in $\text{MoSe}_2/\text{WSe}_2$ HS, where interlayer excitons transform into an electron-hole plasma localized within the individual layers at a photoexcitation density of $\sim 4 \times 10^{12} \text{ cm}^{-2}$, [45]. An abrupt change in the interlayer exciton photoluminescence linewidth has been observed above the MT photoexcitation density [45, 46]. There have been many reports on different heterostructures for carrier relaxation dynamics but primarily for small twist angles [40, 41, 47], with only a few focusing on large twist angles [42]. All these studies are focused on the photoexcitation densities below the MT. This has motivated us to explore the relaxation dynamics above the exciton Mott transition in TMDs HS with large twist angles.

Here, we report the non-degenerate optical pump-optical probe studies of $\text{MoSe}_2/\text{WSe}_2$ HS at different twist angles at ambient conditions. A significant decrease in the recombination time of interlayer electron-hole plasma near the commensurate angles of 21.8° and 38.2° is observed, which is attributed to additional radiative recombination channels arising from Umklapp recombination. Further, the strength of the interlayer Auger recombination is minimum near the commensurate angles. Our present study can help towards the application of type-II HSs in designing optoelectronic devices, namely photovoltaics, photodetectors, and light-emitting devices where charge transfer and recombination times are important

parameters [48].

Experimental details

Non-generate optical pump-optical probe measurements were performed using Ti: Sapphire ultrafast laser system (1 kHz repetition rate, ~ 50 fs pulse width, M/s Spectra-Physics, Spitfire Ace) with the pump and probe energies of 3.1 eV and 1.55 eV, respectively. The pump and probe beams are passed collinearly through an objective lens with the $NA = 0.9$. The spot size of the beam at the sample point was measured to be $\sim 5 \mu\text{m}$. The spot size is the same as the overlapping region of the heterostructure, and the resulting differential reflectivity ($\Delta R/R$) covers the entire overlapping region. Experiments were carried out for different twist angles of $\text{MoSe}_2/\text{WSe}_2$ HS at two pump fluences of 2.0 and 2.8 mJ/cm^2 at room temperature. To investigate carrier relaxation dynamics above the exciton Mott transition, we use a probe beam with a fixed wavelength of 800 nm.

The $\text{MoSe}_2/\text{WSe}_2$ HS were prepared using the chemical vapor deposition method on a *c*-plane sapphire substrate via a two-step process similar to our earlier work [10]. The sapphire substrate were chosen because the strain effects are expected to be minimal (0.08%) compared to silica substrate (0.38%) [49]. The individual monolayers of MoSe_2 and WSe_2 have a triangular geometry as shown in the microscopic image of the sample (Figure 1a). The triangles with light (bright) contrast and bigger (smaller) in size represent WSe_2 (MoSe_2) monolayers as depicted by the black arrows in Figure 1a. A random alignment of triangular-shaped monolayers was obtained as a result of the CVD process, providing us with various twist angles. It has been verified that the TMDs with triangular geometry terminate with transition metal atoms at the edges using transmission electron microscopy [50] and scanning tunneling microscopy [51]. Therefore, the relative orientation of the layers provides us with the angle between the two layers as there is a direct correlation of crystal orientation with the triangular geometry of each monolayer [40, 50, 52]. The twist angle is evaluated as the angle between two lines collinear to the centroid and the vertex of the triangle [53]. One example of evaluating the twist angle is presented in Figure 1b, where red and blue outlined triangles represent MoSe_2 and WSe_2 monolayers, respectively. The lines collinear to the vertex and centroid are the angle bisector in the case of equilateral triangles, which gives the twist angle. The schemes for the front and side view of $\text{MoSe}_2/\text{WSe}_2$ HS for different twist angles are shown elsewhere [10].

Raman characterization

The blue and red shifts of the A_{1g} modes in WS_2 and MoS_2 within their twisted HSs [29] motivated us to perform Raman spectroscopy on HS $MoSe_2/WSe_2$ for various twist angles. The group theory for the individual layer provides the irreducible decomposition of Raman active vibration modes $A_{1g}(R)$, $E_{2g}(R)$, and $E_{1g}(IR+R)$ for MX_2 monolayer [54]. Figure 2a shows the Raman spectrum of the HS region for a twist angle of 49° recorded using 532 nm laser wavelength. We obtain the following vibration modes as shown in Figure 2a: M1($MoSe_2$, A_{1g}): 238.5 cm^{-1} , M2(WSe_2 , $A_{1g}+E_{2g}$): 249 cm^{-1} , M3(WSe_2 , 2LA): 258.5 cm^{-1} , M4($MoSe_2$, E_{2g}): 286 cm^{-1} , M5(WSe_2 , A_2''): 305 cm^{-1} , M6($MoSe_2$, A_2''): 353 cm^{-1} , M7: 373 cm^{-1} and M8: 394 cm^{-1} [55,56]. It confirms the formation of HS with the presence of all the modes of individual monolayers of $MoSe_2$ and WSe_2 . From the perspective of the charge transfer among two vertically stacked monolayers, we concentrate on the out-of-plane modes (A_{1g}) of the two monolayers $MoSe_2$ and WSe_2 stacked together, namely M1 ($MoSe_2$) and M2 (WSe_2).

Figure S1 (supplementary information) shows the Raman spectra of M1, M2, and M3 modes with normalized intensities for different twist angles. The black dashed lines represent the shift of the peak position of modes M1 or M2 at different twist angles. We observed the softening of M1 and hardening of M2 mode for any non-zero twist angle as compared to the aligned geometry. Mode M2 starts stiffening as the twist angle is varied till 17° , followed by softening till 32° and then stiffening again till 39° which is again followed by softening. In a counter behavior, the M1 mode softens as the twist angle is varied till 17° , followed by stiffening till 32° and then softening till 39° , which is again followed by stiffening. The softening and stiffening of the A_{1g} mode (both M1 and M2) depend upon the carrier doping as well as the interlayer coupling [53,57,58]. In transition metal dichalcogenide MoS_2 , increasing the number of layers stiffens the A_{1g} mode and softens the E_{2g} mode due to increased dielectric screening of Coulomb interactions [59,60]. It has been reported that the unidirectional transfer of electrons from monolayer WS_2 to monolayer MoS_2 leads to higher carrier density in MoS_2 and lower carrier density in WS_2 , which can soften or stiffen the respective A_{1g} modes [29]. For the similar staggered bands configuration of HS $MoSe_2/WSe_2$, unidirectional electron flow from WSe_2 to $MoSe_2$ increases (reduces) the carrier density in $MoSe_2$ (WSe_2) and leads to the softening (stiffening) of M1 (M2) modes. To understand the importance of twist angle, we have plotted the difference between the peak position of modes M1 and M2 with twist angles as shown in Figure 2b. Here, the solid blue line shows a systematic variation of the shift of M1 with respect to M2 (or vice-versa) with maximum shift near the commensurate angles of 21.8° and 38.2° . For perfectly aligned HS ($\theta=0^\circ$), the electron transfer and the interlayer coupling

lead to the softening of A_{1g} of both M1 and M2 modes, if we compare these modes in monolayers of MoSe₂ and WSe₂ (Figure S1). However, with a non-zero twist angle, variation in the charge transfer and the interlayer coupling tunes the softening and the corresponding stiffening of M1 and M2 modes and shows an anomalous maximum shift near the commensurate angles. This can be easily understood as the maximum electron transfer and more dielectric screening of Coulomb interaction between electron and hole for the MoSe₂/WSe₂ HS at these specific angles, which are in the vicinity of commensurate angles. We also note the disappearance of M3 (2LA mode of WSe₂) at the twist angles of 19° and 39° as depicted by small arrows in Figure S1 (panel iii), which needs further investigation.

Results and discussions

Figure 3a shows time-resolved differential reflectivity ($\Delta R/R$) for monolayer (ML) MoSe₂ (blue circles), ML WSe₂ (red circles), and HS MoSe₂/WSe₂ at twist angles (θ) of 20° (pink circles) and 35° (black circles) with a fluence of 2.0 mJ/cm². It demonstrates that the relaxation dynamics for the HS differ from those of the individual MLs and vary with different twist angles. For ML MoSe₂, a single exponential decay provides a recombination time of 9.6 ± 0.3 ps, whereas ML WSe₂ exhibits a biexponential decay with recombination times of 1.4 ± 0.15 ps and 20.8 ± 0.5 ps. A biexponential fit for the $\Delta R/R(t)$ (blue circles) for the HS at $\theta=20^\circ$ is shown by solid red curve in Figure 3b, using the equation:

$$\frac{\Delta R}{R}(t) = \frac{1}{2} \left(1 + \text{erf} \left(\frac{t - t_0}{\tau_r} \right) \right) (A_1 e^{-t/\tau_1} + A_2 e^{-t/\tau_2} + A_3) \quad (1)$$

where $(1 + \text{erf}((t - t_0)/\tau_r))$ represents the rise part of the time-resolved $\Delta R/R$, with τ_r being the rise time, which varies in the range of ~ 0.7 -1.0 ps for different twist angles. The fast and slow recombination processes are characterized by amplitudes and recombination times (A_1, τ_1) and (A_2, τ_2), respectively. A_3 is the strength of the slow relaxation process, taken to be constant in the delay time up to 150 ps. Before extracting the fitting parameters for various twist angles, we discuss the mechanism involved in the relaxation dynamics of HS MoSe₂/WSe₂.

Figure 4a shows the type II band alignment in MoSe₂/WSe₂ HS depicting higher energy states of valence band maxima (VBM) and conduction band minima (CBM) of WSe₂ with respect to that of MoSe₂. The optical pump excitation using 400 nm (3.1 eV) laser pulse injects carriers into the conduction band much above the band gap for both constituent monolayers (MoSe₂ $E_g=1.57$ eV, WSe₂ $E_g=1.67$ eV) [61, 62], as shown in the top left panel of Figure 4a. The energetic hot carriers undergo rapid electron-electron scattering and relax to the band edge, followed by a charge transfer between the

MLs, creating both inter and intralayer excitons [34, 35]. However, at a photoexcitation density of 2 mJ/cm² ($n_0 \sim 6.1 \times 10^{14}$ cm⁻²), these interlayer excitons undergo Mott transition, where they transform into a hot electron and hot hole plasma in MoSe₂ and WSe₂ monolayers, respectively [43–46]. These carriers, localized to individual layers, emerge ~ 1 ps after the photoexcitation, when most of the electrons (holes) get transferred to CBM (VBM) of MoSe₂ (WSe₂) [35, 45], as shown in the top right panel of Figure 4a. Localized interlayer charge carriers take longer to recombine compared to intralayer carriers, as the electrons and holes are confined to different layers rather than being in the same monolayer. The bottom left panel of Figure 4a represents the radiative recombination of the intralayer electrons and holes in the individual monolayers, associated with (A_1 , τ_1). For WSe₂/MoSe₂ HS with non-zero twist angle ($4^\circ \pm 2^\circ$), observation of interlayer PL for excitation densities above Mott transition [25, 45] demonstrate the radiative recombination of interlayer electrons and holes, but only at a temperature of 4 K. However, Seyler *et al.* have reported that interlayer electrons and holes in MoSe₂/WSe₂ do not align at $\pm K$ valleys in the first Brillouin zone, emphasizing non-radiative recombination as a dominant process [27]. Therefore, we attribute the slow component of the relaxation dynamics (A_2 , τ_2) to indirect radiative (phonon-mediated) and non-radiative recombination of interlayer electrons and holes, as illustrated in the lower middle panel of Figure 4a. Motivated by the suggestion of non-radiative Auger recombination of interlayer excitons at high excitation densities [63, 64], the A_3 component is attributed to non-radiative interlayer Auger recombination. In this process, electrons and holes from different MLs recombine and transfer the energy to the third particle, such as an electron or a hole, as demonstrated in the lower right panel of Figure 4a.

Figure 5a shows the twist-angle (θ)-dependent behavior of the intralayer photoexcited carriers (A_1) and its recombination time (τ_1) at a fluence of 2.0 mJ/cm². A_1 and τ_1 exhibit no systematic dependence on twist angle as is expected for intralayer carriers recombination in individual monolayers. The recombination dynamics of the interlayer carriers is presented in Figure 5b, where amplitude A_2 is twist-angle independent. The recombination time of interlayer localized electrons and holes, τ_2 (panel ii of Figure 5b) exhibits minima near 20° and 38° . The blue dots represent the data, while the solid blue line is a cubic spline. The component associated with non-radiative Auger recombination of interlayer carriers, A_3 , also shows minima for $\sim 20^\circ$ and $\sim 38^\circ$ (represented by the solid blue line in Figure 5c). The trend of the fitting parameters at a fluence of 2.0 mJ/cm² is similar at a fluence of 2.8 mJ/cm², as shown in supplementary Figure S2.

We offer a qualitative understanding of our results. We observed that τ_2 is maximum at the twist

angle of $\sim 30^\circ$ (Figure 5b), *i.e.* the interlayer localized carriers take the longest time to recombine. This is due to the interlayer distance being maximum at the twist angle of 30° in TMDs HSs [28,29]. Equally interesting is the observation of two minima of τ_2 observed near 20° and 38° . These twist angles are close to the commensurate angles of $\theta = 21.8^\circ$ and 38.2° for MoSe₂/WSe₂ HS, where interlayer localized charge carriers or/and excitons can access an additional channel to recombine [27,30]. Seyler *et al.* have demonstrated that for any non-zero twist angle between two layers, the holes in the valence band of WSe₂ and electrons in the conduction band of MoSe₂ at $\pm K$ points do not align in the first Brillouin zone. However, at the commensurate angle of 21.8° , the valence band and conduction band align at $\pm K$ points in the second Brillouin zone, as shown in Figure 4b, adapted from ref. [27]. At these specific angles, the interlayer charge carriers can recombine radiatively, and the momentum mismatch (due to non-zero twist angle) is compensated by the reciprocal lattice of two layers; the process known as Umklapp recombination [27, 30]. We attribute this Umklapp recombination in the vicinity of commensurate angles as a cause for the two minima observed for τ_2 (Figure 5b). The two different fluences support the evidence of faster relaxation dynamics in the vicinity of commensurate twist angles. The additional radiative recombination channels for interlayer charge carriers result in lesser interlayer charge carriers involved in non-radiative Auger recombination, leading to a trend that shows minima in A_3 near these commensurate angles (Figure 5c). To further investigate the minima for τ_2 near the commensurate angles, the relaxation dynamics is studied as a function of excitation density for different twist angles.

The fluence dependence of the relaxation dynamics of interlayer charge carriers (Figure 5d) shows an increase in interlayer charge carriers with increasing fluence, which saturates beyond 2.0 mJ/cm^2 indicating the threshold of charge transfer in HS MoSe₂/WSe₂ at fluences above 2.0 mJ/cm^2 . It is important to note that τ_2 is least fluence dependent at 20° and 38° in comparison to other twist angles, despite a significant increase in the number of interlayer charge carriers. Intralayer charge carriers do not exhibit this distinct behavior near commensurate angles, as shown by the fluence dependence of amplitude A_1 and τ_1 in supplementary Figure S3. In conclusion, the additional recombination channels for interlayer charge carriers at commensurate angles demonstrate the fluence independence of recombination time (τ_2) within the reported range up to 2.8 mJ/cm^2 .

Conclusions

In summary, we have reported the optical pump optical probe spectroscopy of $\text{MoSe}_2/\text{WSe}_2$ HS with different twist angles at high excitation densities above the Mott transition. We observed a significant decrease in interlayer exciton recombination time in the proximity of commensurate angles of 21.8° and 38.2° . We interpret the result as a consequence of the availability of new radiative recombination channels due to Umklapp recombination. The least fluence dependence of interlayer charge carriers recombination time near commensurate angles further supports the presence of additional recombination channels. Our results can be helpful in designing the applications of twisted vdW HS in optoelectronic applications.

Acknowledgments

AKS thanks the Department of Science and Technology, Government of India, for its financial support under the National Science Chair Professorship and Nanomission (Grant No. DST/NM/TUE/QM-5/2019). DVSM also acknowledges the DST for the Nanomission grant. VA acknowledges CSIR for the research fellowship. PKN acknowledges the MHRD STARS research grant [STARS/APR2019/396] and the support from the Institute of Eminence scheme at IIT-Madras through the 2D Materials Research and Innovation Group.

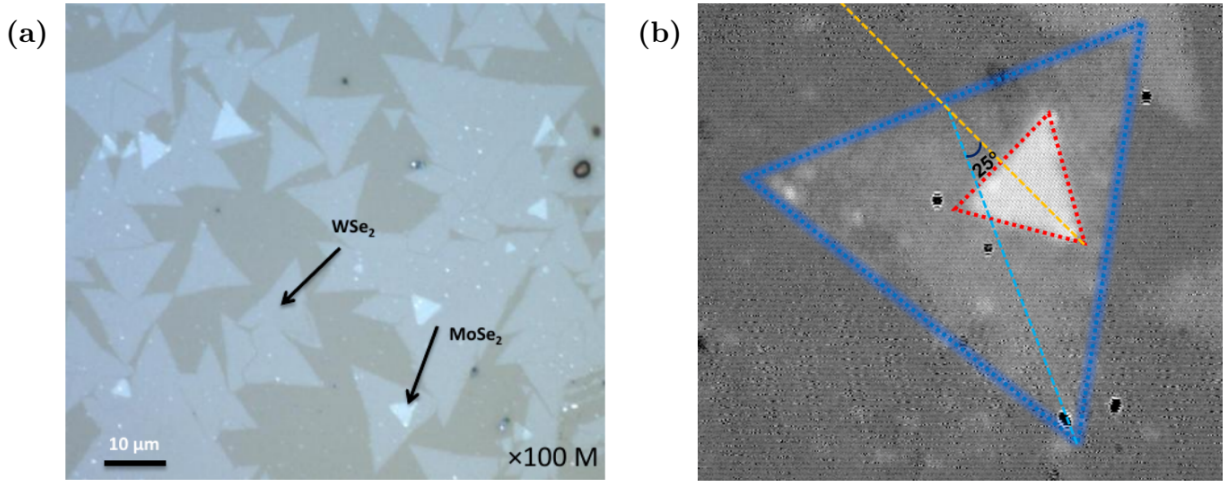


Figure 1: (a) Microscopic image of $\text{MoSe}_2/\text{WSe}_2$ HS depicting WSe_2 as a bottom layer (big triangles) with dull contrast and MoSe_2 as a top layer (smaller triangles) with brighter contrast, (b) Angle evaluation between two monolayers with the blue(red) triangle as a boundary of $\text{WSe}_2(\text{MoSe}_2)$ monolayers.

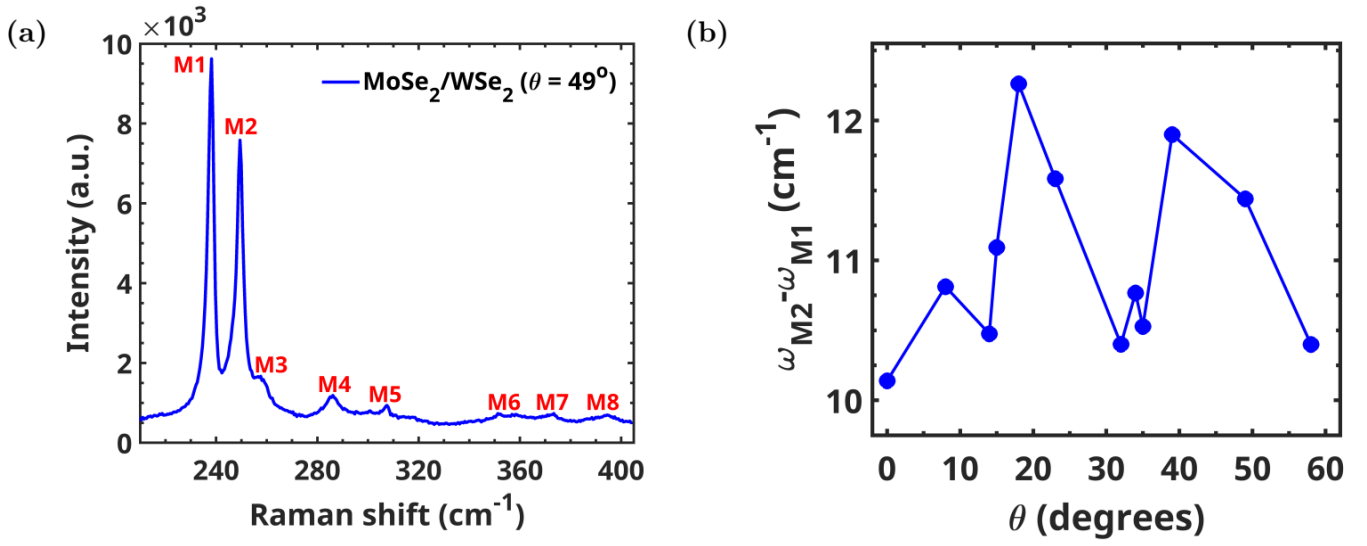


Figure 2: (a) The Raman spectrum for HS at a $\theta = 49^\circ$. M1(M2) represents the A_{1g} mode of $\text{MoSe}_2(\text{WSe}_2)$, The respective modes are as follows: M1(238.5 cm^{-1}), M2(249 cm^{-1}), M3(258.5 cm^{-1}), M4(286 cm^{-1}), M5(305 cm^{-1}), M6(353 cm^{-1}), M7(373 cm^{-1}), M8(394 cm^{-1}). (b) The difference of frequencies of modes M1 and M2 is presented with twist angles. The difference is maximum in the proximity of commensurate angles of 21.8° and 38.2°. The error bars are smaller than the symbols representing the data points.

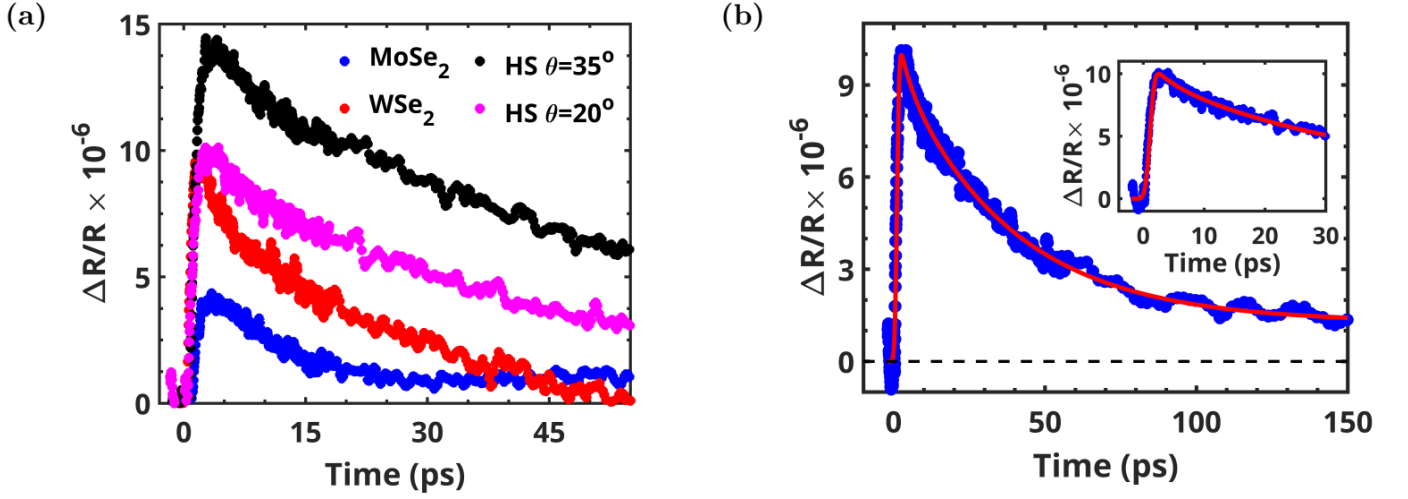


Figure 3: (a) Time evolution of $\Delta R/R$ for ML MoSe₂ (blue circles), ML WSe₂ (red circles), HS MoSe₂/WSe₂ at $\theta=20^\circ$ (pink circles), $\theta=35^\circ$ (black circles). (b) The differential reflectivity $\Delta R/R$ for HS MoSe₂/WSe₂ at twist angle of $\theta=20^\circ$ (blue circles) is fitted using Eq.(1) (red solid line). The inset shows the fit of the experimental data up to 30 ps.

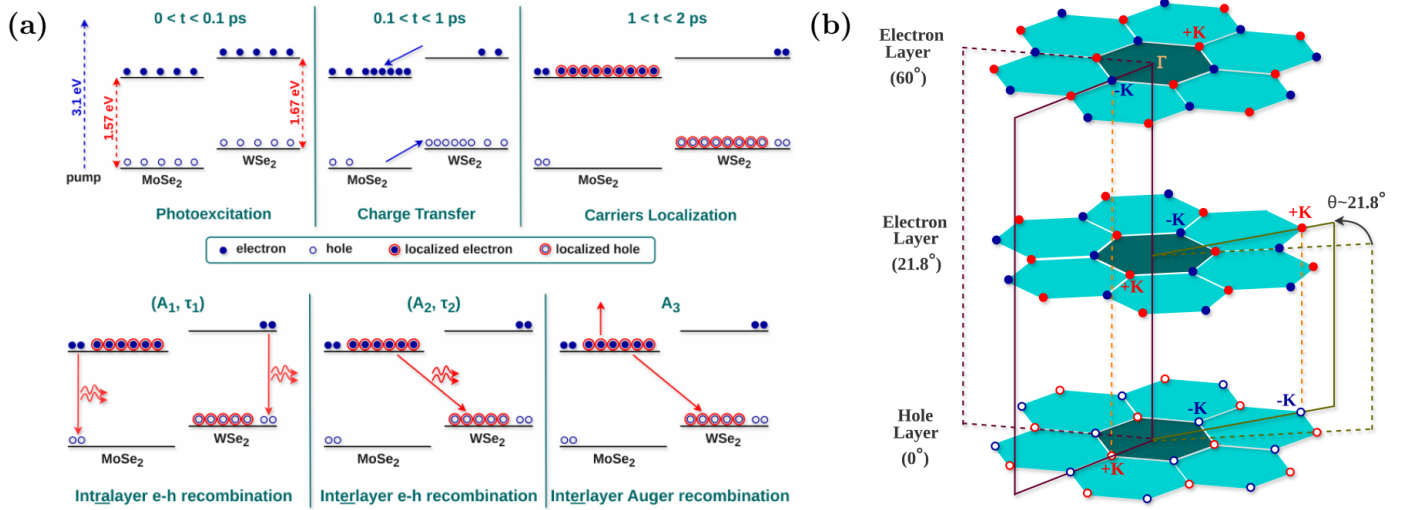


Figure 4: Type II band structure of HS MoSe₂/WSe₂, (a) Top panel: Photoexcitation: Electrons are transferred to the conduction band of MoSe₂ and WSe₂, Charge transfer: electrons (holes) transfer from conduction (valence) band of WSe₂ (MoSe₂) to MoSe₂ (WSe₂), Carriers Localization: interlayer charge carriers localized to distinct individual layers. Bottom panel: intralayer e-h recombination (A_1, τ_1): electrons and holes within the same layer recombine radiatively, Interlayer e-h recombination (A_2, τ_2): Electron and holes in different layers recombine radiatively, Interlayer Auger recombination (A_3): Electrons and holes in distinct layers recombine non-radiatively, transferring energy to a third particle, which is either an electron or a hole. (b) A schematic representation for the valley alignments in the extended Brillouin zone for a twisted HS: The solid and open dots represent the -K(blue) and +K(red) valleys in the electron and hole layers. For a twist angle of $\sim 21.8^\circ$, the valleys +K, -K and -K, +K align in the second Brillouin zone (indicated by an orange dashed line from the middle layer to the bottom layer), which has the same valley pairing for the 60° twisted HS (denoted by the orange dashed line from the top layer to the bottom layers). Adapted from *Seyler et al.* [27].

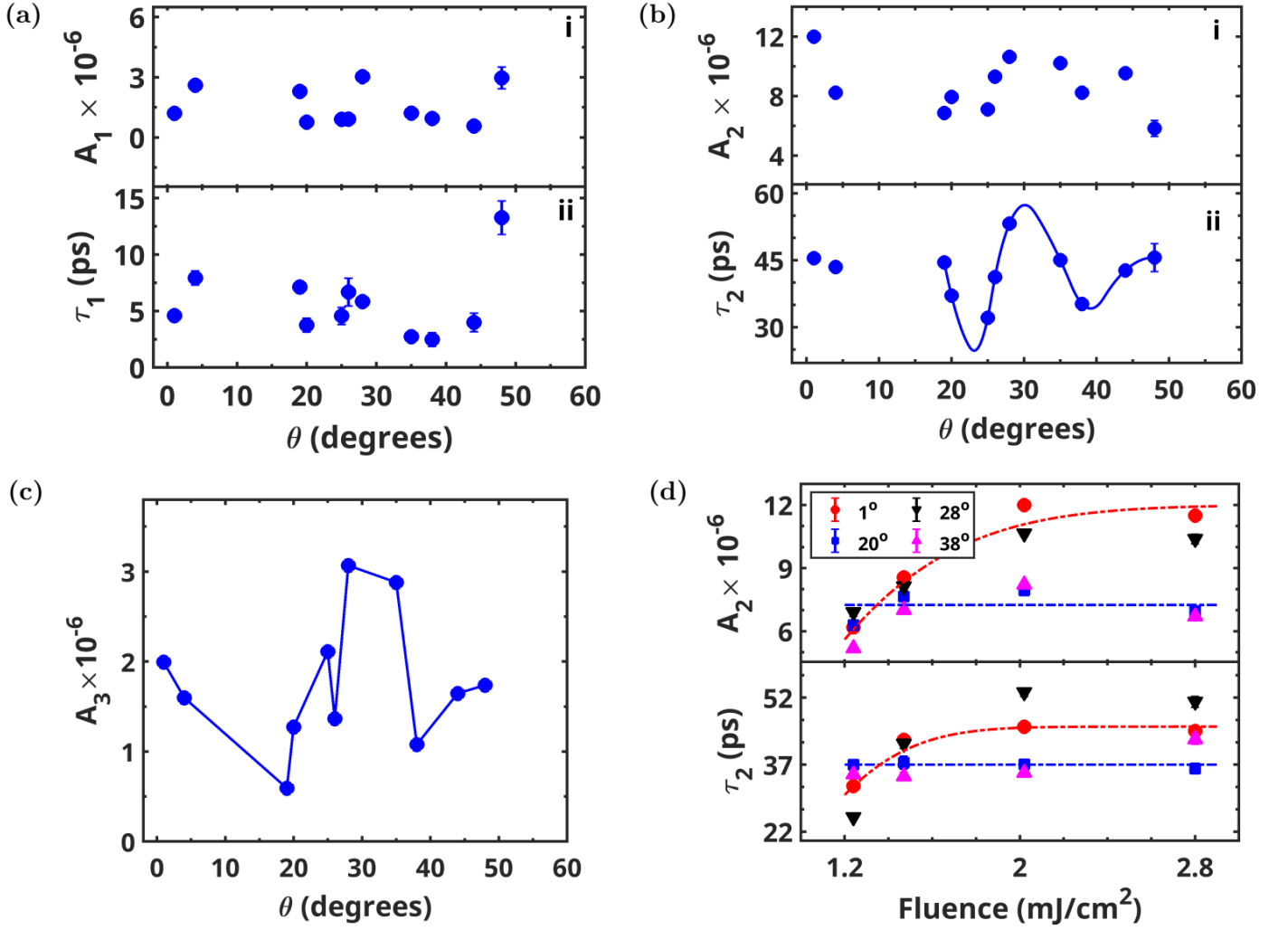


Figure 5: Twist-angle dependence of (a) amplitude (A_1) and recombination time (τ_1), (b) amplitude (A_2) and recombination time (τ_2), the solid blue line represents a cubic spline. (c) amplitude (A_3) at a fluence of 2.0 mJ/cm². (d) Fluence dependence of amplitude (A_2) and recombination time (τ_2) for different twist angles. The dashed and dotted (red and blue) lines are guides to the eyes for the data corresponding to 1° and 20°. The error bars are smaller than the symbols representing the data points.

References

- [1] Alexey Chernikov, Timothy C. Berkelbach, Heather M. Hill, Albert Rigosi, Yilei Li, Burak Aslan, David R. Reichman, Mark S. Hybertsen, and Tony F. Heinz. Exciton binding energy and nonhydrogenic rydberg series in monolayer WS_2 . *Phys. Rev. Lett.*, **113**:076802, (2014).
- [2] Keliang He, Nardeep Kumar, Liang Zhao, Zefang Wang, Kin Fai Mak, Hui Zhao, and Jie Shan. Tightly bound excitons in monolayer WSe_2 . *Phys. Rev. Lett.*, **113**:026803, (2014).
- [3] Yuanyuan Li, Qiannan Cui, Frank Ceballos, Samuel D. Lane, Zeming Qi, and Hui Zhao. Ultrafast interlayer electron transfer in incommensurate transition metal dichalcogenide homobilayers. *Nano Letters*, **17**(11):6661–6666, (2017).
- [4] Nardeep Kumar, Sina Najmaei, Qiannan Cui, Frank Ceballos, Pulickel M. Ajayan, Jun Lou, and Hui Zhao. Second harmonic microscopy of monolayer MoS_2 . *Phys. Rev. B*, **87**:161403, (2013).
- [5] Yilei Li, Yi Rao, Kin Fai Mak, Yumeng You, Shuyuan Wang, Cory R. Dean, and Tony F. Heinz. Probing symmetry properties of few-layer MoS_2 and h-BN by optical second-harmonic generation. *Nano Letters*, **13**(7):3329–3333, (2013).
- [6] Leandro M. Malard, Thonimar V. Alencar, Ana Paula M. Barboza, Kin Fai Mak, and Ana M. de Paula. Observation of intense second harmonic generation from MoS_2 atomic crystals. *Phys. Rev. B*, **87**:201401, (2013).
- [7] Hualing Zeng, Junfeng Dai, Wang Yao, Di Xiao, and Xiaodong Cui. Valley polarization in MoS_2 monolayers by optical pumping. *Nature Nanotechnology*, **7**:490–493, (2012).
- [8] Kin Fai Mak, Keliang He, Jie Shan, and Tony F. Heinz. Control of valley polarization in monolayer MoS_2 by optical helicity. *Nature Nanotechnology*, **7**:494–498, (2012).
- [9] Cheng Gong, Hengji Zhang, Weihua Wang, Luigi Colombo, Robert M. Wallace, and Kyeongjae Cho. Band alignment of two-dimensional transition metal dichalcogenides: Application in tunnel field effect transistors. *Applied Physics Letters*, **103**(5):053513, (2013).
- [10] Pramoda K. Nayak, Yevhen Horbatenko, Seongjoon Ahn, Gwangwoo Kim, Jae-Ung Lee, Kyung Yeol Ma, A-Rang Jang, Hyunseob Lim, Dogyeong Kim, Sunmin Ryu, Hyeonsik Cheong, Noejung Park, and Hyeon Suk Shin. Probing evolution of twist-angle-dependent interlayer excitons in $\text{MoSe}_2/\text{WSe}_2$ van der waals heterostructures. *ACS Nano*, **11**(4):4041–4050, (2017).

- [11] Torben L. Purz, Eric W. Martin, Pasqual Rivera, William G. Holtzmann, Xiaodong Xu, and Steven T. Cundiff. Coherent exciton-exciton interactions and exciton dynamics in a MoSe₂/WSe₂ heterostructure. *Phys. Rev. B*, **104**:L241302, (2021).
- [12] John R. Schaibley. Control of interlayer valley excitons in atomically-thin MoSe₂-WSe₂ heterostructures. In *OPTO*, (2017).
- [13] Yan Zeng, Wei Dai, Rundong Ma, Zhe Li, Zhenwei Ou, Cheng Wang, Yiling Yu, Tong Zhu, Xiaoze Liu, Ti Wang, and Hongxing Xu. Distinguishing ultrafast energy transfer in atomically thin MoS₂/WS₂ heterostructures. *Small*, **18**(44):2204317, (2022).
- [14] Kha Tran, Galan Moody, Fengcheng Wu, Xiaobo Lu, Junho Choi, Kyoungwan Kim, Amritesh Rai, Daniel A. Sanchez, Jiamin Quan, Akshay Singh, Jacob Embley, André Zepeda, Marshall Campbell, Travis Autry, Takashi Taniguchi, Kenji Watanabe, Nanshu Lu, Sanjay K. Banerjee, Kevin L. Silverman, Suenne Kim, Emanuel Tutuc, Li Yang, Allan H. MacDonald, and Xiaoqin Li. Evidence for moiré excitons in van der waals heterostructures. *Nature*, **567**(7746):71–75, (2019).
- [15] Chenhao Jin, Emma C. Regan, Aiming Yan, M. Iqbal Bakti Utama, Danqing Wang, Sihan Zhao, Ying Qin, Sijie Yang, Zhiren Zheng, Shenyang Shi, Kenji Watanabe, Takashi Taniguchi, Sefaattin Tongay, Alex Zettl, and Feng Wang. Observation of moiré excitons in WSe₂/WS₂ heterostructure superlattices. *Nature*, **567**(7746):76–80, (2019).
- [16] James G. McHugh, Vladimir V. Enaldiev, and Vladimir I. Fal’ko. Moiré superstructures in marginally twisted NbSe₂ bilayers. *Phys. Rev. B*, **108**:224111, Dec (2023).
- [17] Niclas Götting, Frederik Lohof, and Christopher Gies. Moiré-bose-hubbard model for interlayer excitons in twisted transition metal dichalcogenide heterostructures. *Phys. Rev. B*, **105**:165419, (2022).
- [18] Zidong Li, Xiaobo Lu, Darwin F. Cordovilla Leon, Zhengyang Lyu, Hongchao Xie, Jize Hou, Yanzhao Lu, Xiaoyu Guo, Austin Kaczmarek, Takashi Taniguchi, Kenji Watanabe, Liuyan Zhao, Li Yang, and Parag B. Deotare. Interlayer exciton transport in MoSe₂/WSe₂ heterostructures. *ACS Nano*, **15**(1):1539–1547, (2021).
- [19] Michael Förg, Anvar S. Baimuratov, Stanislav Yu. Kruchinin, Ilia A. Vovk, Johannes Scherzer, Jonathan Förste, Victor Funk, Kenji Watanabe, Takashi Taniguchi, and Alexander Högele. Moiré

- excitons in MoSe₂-WSe₂ heterobilayers and heterotrilayers. *Nature Communications*, **12**:1656, (2021).
- [20] V. V. Enaldiev, F. Ferreira, J. G. McHugh, and Vladimir I. Fal'ko. Self-organized quantum dots in marginally twisted MoSe₂/WSe₂ and MoS₂/WS₂ bilayers. *npj 2D Materials and Applications*, **6**(1):74, (2022).
- [21] Long Zhang, Zhe Zhang, Fengcheng Wu, Danqing Wang, Rahul Gogna, Shaocong Hou, Kenji Watanabe, Takashi Taniguchi, Krishnamurthy Kulkarni, Thomas Kuo, Stephen R. Forrest, and Hui Deng. Twist-angle dependence of moiré excitons in WS₂/MoSe₂ heterobilayers. *Nature Communications*, **11**(1):5888, (2020).
- [22] Zhiming Zhang, Yimeng Wang, Kenji Watanabe, Takashi Taniguchi, Keiji Ueno, Emanuel Tutuc, and Brian J. LeRoy. Flat bands in twisted bilayer transition metal dichalcogenides. *Nature Physics*, **16**(11):1093–1096, (2020).
- [23] Trithep Devakul, Valentin Crépel, Yang Zhang, and Liang Fu. Magic in twisted transition metal dichalcogenide bilayers. *Nature Communications*, **12**(1):6730, (2021).
- [24] Mit H. Naik and Manish Jain. Ultraflatbands and shear solitons in Moiré patterns of twisted bilayer transition metal dichalcogenides. *Phys. Rev. Lett.*, **121**:266401, (2018).
- [25] Chirag Chandrakant Palekar, Joakim Hagel, Barbara Rosa, Samuel Brem, Ching-Wen Shih, Imad Limame, Martin von Helversen, Sefaattin Tongay, Ermin Malic, and Stephan Reitzenstein. Anomalous redshift in interlayer exciton emission with increasing twist angle in WSe₂/MoSe₂ heterostructures. *2D Materials*, **11**(2):025034, (2024).
- [26] Kai Wang, Bing Huang, Mengkun Tian, Frank Ceballos, Ming-Wei Lin, Masoud Mahjouri-Samani, Abdelaziz Boulesbaa, Alexander A. Purotzky, Christopher M. Rouleau, Mina Yoon, Hui Zhao, Kai Xiao, Gerd Duscher, and David B. Geohegan. Interlayer coupling in twisted WSe₂/WS₂ bilayer heterostructures revealed by optical spectroscopy. *ACS Nano*, **10**(7):6612–6622, (2016).
- [27] Kyle L. Seyler, Pasqual Rivera, Hongyi Yu, Nathan P. Wilson, Essance L. Ray, David G. Mandrus, Jiaqiang Yan, Wang Yao, and Xiaodong Xu. Signatures of moiré-trapped valley excitons in MoSe₂/WSe₂ heterobilayers. *Nature*, **567**:66–70, (2019).

- [28] Ke Wu, Hongxia Zhong, Quanbing Guo, Jibo Tang, Jing Zhang, Lihua Qian, Zhifeng Shi, Chendong Zhang, Shengjun Yuan, Shunping Zhang, and Hongxing Xu. Identification of twist-angle-dependent excitons in WS_2/WSe_2 . *National Science Review*, **9**, (2021).
- [29] Lishu Wu, Chunxiao Cong, Jingzhi Shang, Weihuang Yang, Yu Chen, Jiadong Zhou, Wei Ai, Yanlong Wang, Shun Feng, Hongbo Zhang, Zheng Liu, and Ting Yu. Raman scattering investigation of twisted WS_2/MoS_2 heterostructures: interlayer mechanical coupling versus charge transfer. *Nano Research*, **14**:2215–2223, (2021).
- [30] Hongyi Yu, Yong Wang, Qingjun Tong, Xiaodong Xu, and Wang Yao. Anomalous light cones and valley optical selection rules of interlayer excitons in twisted heterobilayers. *Phys. Rev. Lett.*, **115**:187002, (2015).
- [31] Hanping Xiong, Xianhua Nie, Li Zhao, and Shuai Deng. Engineering symmetry breaking in twisted $\text{MoS}_2/\text{MoSe}_2$ heterostructures for optimal thermoelectric performance. *ACS Applied Materials & Interfaces*, **16**(19):25124–25135, (2024). PMID: 38709893.
- [32] Saurav Sachin, Puja Kumari, Neelam Gupta, Shivani Rani, Subhasmita Kar, and Soumya Jyoti Ray. Van der waals twistronics in a MoS_2/WS_2 heterostructure. *Computational Condensed Matter*, **35**:e00797, (2023).
- [33] Amalya C. Johnson, Johnathan D. Georgaras, Xiaozhe Shen, Helen Yao, Ashley P. Saunders, Helen J. Zeng, Hyungjin Kim, Aditya Sood, Tony F. Heinz, Aaron M. Lindenberg, Duan Luo, Felipe H. da Jornada, and Fang Liu. Hidden phonon highways promote photoinduced interlayer energy transfer in twisted transition metal dichalcogenide heterostructures. *Science Advances*, **10**(4):eadj8819, (2024).
- [34] Xiaoping Hong, Jonghwan Kim, Su-Fei Shi, Yu Zhang, Chenhao Jin, Yinghui Sun, Sefaattin Tongay, Junqiao Wu, Yanfeng Zhang, and Feng Wang. Ultrafast charge transfer in atomically thin MoS_2/WS_2 heterostructures. *Nature Nanotechnology*, **9**(9):682–686, (2014).
- [35] Frank Ceballos, Matthew Z. Bellus, Hsin-Ying Chiu, and Hui Zhao. Ultrafast charge separation and indirect exciton formation in a MoS_2 - MoSe_2 van der waals heterostructure. *ACS Nano*, **8**(12):12717–12724, (2014).
- [36] Frank Ceballos, Matthew Z. Bellus, Hsin-Ying Chiu, and Hui Zhao. Probing charge transfer excitons in a MoSe_2 - WS_2 van der waals heterostructure. *Nanoscale*, **7**:17523–17528, (2015).

- [37] Bo Peng, Yu Guannan, Liu Xinfeng, Bo Liu, Xiao Liang, Lei Bi, Longjiang Deng, Tze Chien Sum, and Kian Ping Loh. Ultrafast charge transfer in MoS₂/WSe₂ p–n heterojunction. *2D Materials*, **3**(2):025020, (2016).
- [38] Peymon Zereschki, Yaqing Wei, Run Long, and Hui Zhao. Layer-coupled states facilitate ultrafast charge transfer in a transition metal dichalcogenide trilayer heterostructure. *The Journal of Physical Chemistry Letters*, **9**(20):5970–5978, (2018).
- [39] R. Krause, S. Aeschlimann, M. Chávez-Cervantes, R. Perea-Causin, S. Brem, E. Malic, S. Forti, F. Fabbri, C. Coletti, and I. Gierz. Microscopic understanding of ultrafast charge transfer in van der waals heterostructures. *Phys. Rev. Lett.*, **127**:276401, (2021).
- [40] Ziheng Ji, Hao Hong, Jin Zhang, Qi Zhang, Wei Huang, Ting Cao, Ruixi Qiao, Can Liu, Jing Liang, Chuanhong Jin, Liying Jiao, Kebin Shi, Sheng Meng, and Kaihui Liu. Robust stacking-independent ultrafast charge transfer in MoS₂/WS₂ bilayers. *ACS Nano*, **11**(12):12020–12026, (2017).
- [41] Jin Zhang, Hao Hong, Chao Lian, Wei Ma, Xiaozhi Xu, Xu Zhou, Huixia Fu, Kaihui Liu, and Sheng Meng. Interlayer-state-coupling dependent ultrafast charge transfer in MoS₂/WS₂ bilayers. *Advanced Science*, **4**(9):1700086, (2017).
- [42] Haiming Zhu, Jue Wang, Zizhou Gong, Young Duck Kim, James Hone, and X.-Y. Zhu. Interfacial charge transfer circumventing momentum mismatch at two-dimensional van der Waals heterojunctions. *Nano Letters*, **17**(6):3591–3598, (2017).
- [43] E. Hendry, M. Koeberg, and M. Bonn. Exciton and electron-hole plasma formation dynamics in ZnO. *Phys. Rev. B*, **76**:045214, (2007).
- [44] Gabija Kiršanskė, Petru Tighineanu, Raphaël S. Daveau, Javier Miguel-Sánchez, Peter Lodahl, and Søren Stobbe. Observation of the exciton Mott transition in the photoluminescence of coupled quantum wells. *Phys. Rev. B*, **94**:155438, (2016).
- [45] Jue Wang, Jenny Ardelean, Yusong Bai, Alexander Steinhoff, Matthias Florian, Frank Jahnke, Xiaodong Xu, Mackillo Kira, James Hone, and X.-Y. Zhu. Optical generation of high carrier densities in 2D semiconductor heterobilayers. *Science Advances*, **5**(9):eaax0145, (2019).
- [46] M. Stern, V. Garmider, V. Umansky, and I. Bar-Joseph. Mott transition of excitons in coupled quantum wells. *Phys. Rev. Lett.*, **100**:256402, (2008).

- [47] Albert F. Rigosi, Heather M. Hill, Yilei Li, Alexey Chernikov, and Tony F. Heinz. Probing interlayer interactions in transition metal dichalcogenide heterostructures by optical spectroscopy: MoS₂/WS₂ and MoSe₂/WSe₂. *Nano Letters*, **15**(8):5033–5038, (2015).
- [48] Yuan Liu, Nathan O. Weiss, Xidong Duan, Hung-Chieh Cheng, Yu Huang, and Xiangfeng Duan. Van der waals heterostructures and devices. *Nature Reviews Materials*, **1**(9):16042, (2016).
- [49] Hang Xin, Jingyun Zhang, Cuihong Yang, and Yunyun Chen. Direct detection of inhomogeneity in cvd-grown 2d tmd materials via k-means clustering raman analysis. *Nanomaterials*, **12**(3), 2022.
- [50] A M van der Zande, P Y Huang, D A Chenet, T C Berkelbach, Y You, G H Lee, T F Heinz, D R Reichman, D A Muller, and J C Hone. Exploring atomic defects in molybdenum disulphide monolayers. *Nature materials*, **12**:554–561, (2013).
- [51] Jeppe V. Lauritsen, Jakob Kibsgaard, Stig Helveg, Henrik Topsøe, Bjerne S. Clausen, Erik Lægsgaard, and Flemming Besenbacher. Size-dependent structure of MoS₂ nanocrystals. *Nature Nanotechnology*, **2**(1):53–58, (2007).
- [52] Xu Zhou, Jingxin Cheng, Yubing Zhou, Ting Cao, Hao Hong, Zhimin Liao, Shiwei Wu, Hailin Peng, Kaihui Liu, and Dapeng Yu. Strong second-harmonic generation in atomic layered GaSe. *Journal of the American Chemical Society*, **137**(25):7994–7997, (2015).
- [53] Kaihui Liu, Liming Zhang, Ting Cao, Chenhao Jin, Diana Qiu, Qin Zhou, Alex Zettl, Peidong Yang, Steve G. Louie, and Feng Wang. Evolution of interlayer coupling in twisted molybdenum disulfide bilayers. *Nature Communications*, **5**:4966, (2014).
- [54] Mei Yang, Xuerui Cheng, Yuanyuan Li, Yufen Ren, Miao Liu, and Zeming Qi. Anharmonicity of monolayer MoS₂, MoSe₂, and WSe₂: A Raman study under high pressure and elevated temperature. *Applied Physics Letters*, **110**(9):093108, (2017).
- [55] Woosuk Choi, Imtisal Akhtar, Malik Abdul Rehman, Minwook Kim, Dongwoon Kang, Jongwan Jung, Yoon Myung, Jungcheol Kim, Hyeonsik Cheong, and Yongho Seo. Twist-angle-dependent optoelectronics in a few-layer transition-metal dichalcogenide heterostructure. *ACS Applied Materials & Interfaces*, **11**(2):2470–2478, (2019).
- [56] Lama Khalil, Debora Pierucci, Emilio Velez-Fort, José Avila, Céline Vergnaud, and Pavel Dudin. Hybridization and localized flat band in the WSe₂/MoSe₂ heterobilayer. *Nanotechnology*, **34**:045702, (2023).

- [57] Xin Zhang, Xiao-Fen Qiao, Wei Shi, Jiang-Bin Wu, De-Sheng Jiang, and Ping-Heng Tan. Phonon and raman scattering of two-dimensional transition metal dichalcogenides from monolayer, multi-layer to bulk material. *Chem. Soc. Rev.*, **44**:2757–2785, (2015).
- [58] Biswanath Chakraborty, Achintya Bera, D. V. S. Muthu, Somnath Bhowmick, U. V. Waghmare, and A. K. Sood. Symmetry-dependent phonon renormalization in monolayer MoS₂ transistor. *Phys. Rev. B*, **85**:161403, (2012).
- [59] Changgu Lee, Hugen Yan, Louis E. Brus, Tony F. Heinz, James Hone, and Sunmin Ryu. Anomalous lattice vibrations of single and few-layer MoS₂. *ACS Nano*, **4**(5):2695–2700, (2010).
- [60] A. Molina-Sánchez and L. Wirtz. Phonons in single-layer and few-layer MoS₂ and WS₂. *Phys. Rev. B*, **84**:155413, (2011).
- [61] Xin Lu, M. Iqbal Bakti Utama, Junhao Lin, Xue Gong, Jun Zhang, Yanyuan Zhao, Sokrates T. Pantelides, Jingxian Wang, Zhili Dong, Zheng Liu, Wu Zhou, and Qihua Xiong. Large-area synthesis of monolayer and few-layer MoSe₂ films on SiO₂ substrates. *Nano Letters*, **14**(5):2419–2425, (2014).
- [62] Jing-Kai Huang, Jiang Pu, Chang-Lung Hsu, Ming-Hui Chiu, Zhen-Yu Juang, Yung-Huang Chang, Wen-Hao Chang, Yoshihiro Iwasa, Taishi Takenobu, and Lain-Jong Li. Large-area synthesis of highly crystalline WSe₂ monolayers and device applications. *ACS Nano*, **8**(1):923–930, (2014).
- [63] J. Binder, J. Howarth, F. Withers, M. R. Molas, T. Taniguchi, K. Watanabe, C. Faugeras, A. Wysmolek, M. Danovich, V. I. Fal’ko, A. K. Geim, K. S. Novoselov, M. Potemski, and A. Kozikov. Upconverted electroluminescence via Auger scattering of interlayer excitons in van der Waals heterostructures. *Nature Communications*, **10**(1):2335, (2019).
- [64] Cheng-Syuan Cai, Wei-Yan Lai, Po-Hsuan Liu, Tzu-Chieh Chou, Ro-Ya Liu, Chih-Ming Lin, Shangjr Gwo, and Wei-Ting Hsu. Ultralow Auger-assisted interlayer exciton annihilation in WS₂/WSe₂ Moiré heterobilayers. *Nano Letters*, **24**(9):2773–2781, (2024).

Twist Angle Dependent Ultrafast Transient Dynamics of MoSe₂/WSe₂ van der Waals Heterostructures beyond the Exciton Mott Transition

Vikas Arora^{1,2}, Pramoda K Nayak^{3,4}, D. V. S. Muthu¹, A K Sood^{*1,2}

June 12, 2025

¹*Department of Physics, Indian Institute of Science, Bangalore 560012, India*

²*Centre for Ultrafast Laser Applications, Indian Institute of Science, Bangalore 560012, India*

³*2D Materials Research and Innovation Group, Department of Physics, Indian Institute of Technology
Madras, Chennai 600036, India*

⁴*Centre for Nano and Materials Sciences, Jain (Deemed-to-be University), Jain Global Campus,
Kanakpura, Bangalore 562112, Karnataka, India*

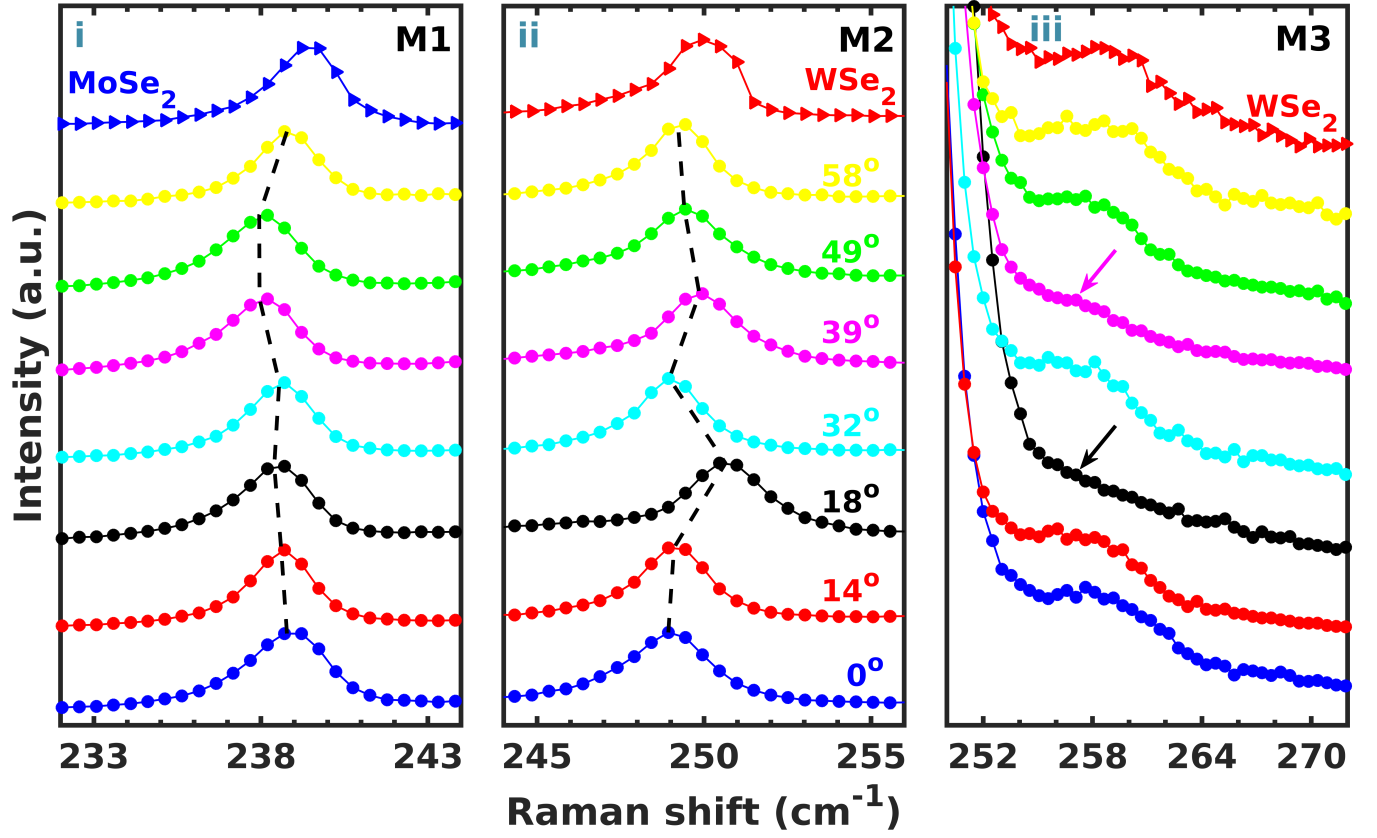


Figure S1: The graphs depict (i) M1, (ii) M2 and (iii) M3 modes at different twist angles and constituent monolayers. The corresponding softening and stiffening of M1 and M2 modes with the twist angle are indicated by the black dashed line, M3 mode disappears at $\theta=18^\circ$ and 39° as indicated by solid arrows in panel iii.

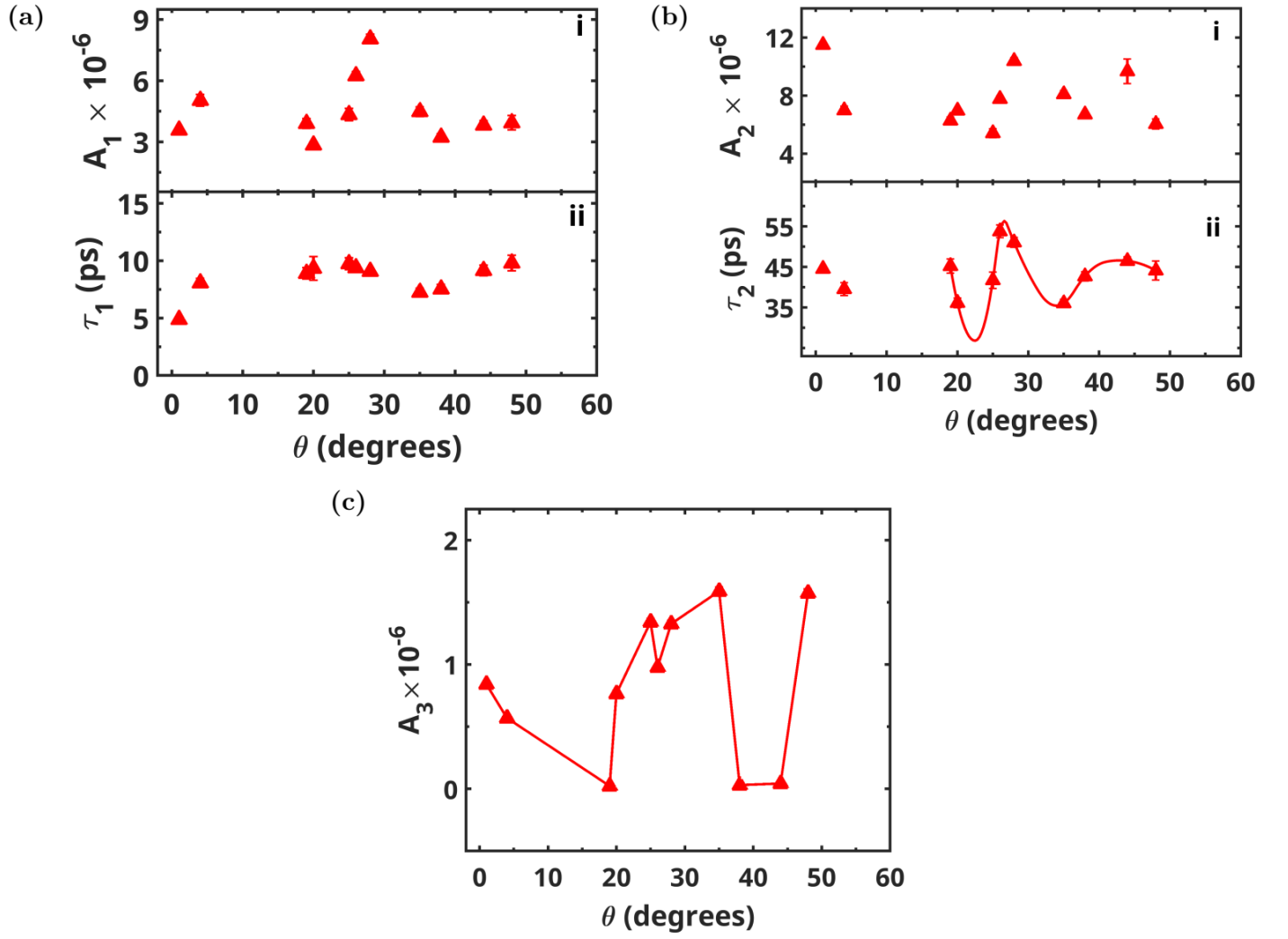


Figure S2: Amplitude and recombination time: (a) (A_1 , τ_1), (b) (A_2 , τ_2), (c) amplitude (A_3) as a function of twist angle at a fluence of 2.8 mJ/cm².

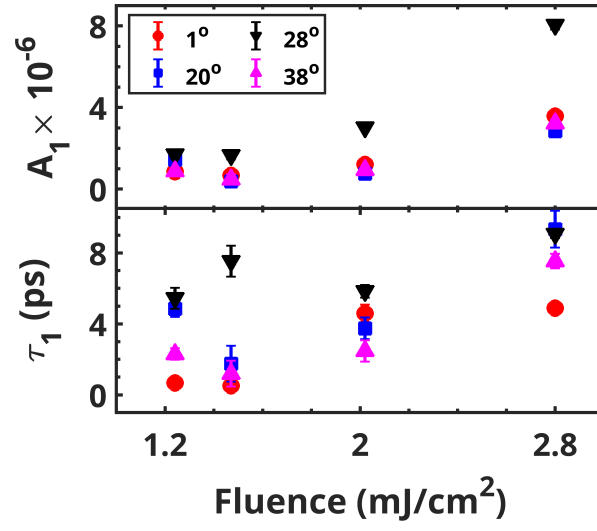


Figure S3: Fluence dependence of amplitude A_1 and relaxation time τ_1 at different twist angles.